Synthesis and characterisation of low valent Mn-complexes as models for Mn-catalases†

Gustav Berggren,[a] Ping Huang,[a] Lars Eriksson,[b] Stenbjörn Styring,[a] Magnus F. Anderlund[a] and Anders Thapper*[a]

Received 18th March 2010, Accepted 12th August 2010
DOI: 10.1039/c0dt00165a

In this work we report the synthesis of two novel manganese complexes, [**L1**$_3$Mn$^{II}_6$](ClO$_4$)$_6$ (**1**·(ClO$_4$)$_6$) and [**L2**Mn$^{II}_2$(μ-OAc)(μ-Cl)](ClO$_4$)$_2$ (**2**·(ClO$_4$)$_2$), where **L1**$^{2-}$ is the 2,2′-(1,3-phenylenebis(methylene))bis-((2-(bis(pyridin-2-ylmethyl)amino)ethyl)azanediyl)diacetic acid anion and **L2** is *N1*,*N1*′-(1,3-phenylenebis(methylene))bis(*N2*,*N2*′-bis(pyridin-2-ylmethyl)ethane-1,2-diamine). The ligands Na$_2$**L1** and **L2** are built on the same backbone, **L2** only contains nitrogen donors, while two carboxylate arms have been introduced in Na$_2$**L1**. The two complexes have been characterized by single-crystal X-ray diffraction, magnetic susceptibility, EPR spectroscopy, and electrochemistry. X-Ray crystallography revealed that **1** is a manganese(II) hexamer and **2** is a manganese(II) dimer featuring an unprecedented mono-μ-acetato, mono-μ-chlorido bridging motif. The ability of the complexes to catalyse H_2O_2 disproportionation, thereby acting as models for manganese catalases, has been investigated and compared to the activity of two other related manganese complexes. The introduction of carboxylate donors in the ligands, leading to increased denticity, resulted in a drop in H_2O_2 disproportionation activity.

Introduction

Manganese ions are present in the active sites of a number of redox active enzymes such as the oxygen-evolving complex of photosystem II, manganese catalases, and manganese superoxide dismutases.[1] The manganese catalases (MnCat) are a group of enzymes that protect living organisms from the deleterious effects of H_2O_2.[2,3] The active site in MnCat consists of two manganese ions coordinated by histidine and glutamate side chains.[4,5] Two prominent features of the active site are challenging to model with biomimetic complexes. The first is the asymmetric nature of the dinuclear site, where one of the manganese ions is six coordinate while the other is five coordinate and therefore more accessible for the substrate (*i.e.* H_2O_2). The other is the presence of multiple types of manganese–carboxylate interaction modes. The three glutamate side chains act like a bridging bidentate, a non-bridging bidentate, and a monodentate ligand respectively to the manganese ions. Even though there has recently been an increased interest in manganese–carboxylate chemistry,[6–9] and a large number of model systems for MnCat have been reported,[10] only a limited number of studies have approached asymmetric complexes with carboxylate donors or complexes with several different carboxylate donors.[11–13]

As dinucleating ligands provide a straightforward route to asymmetric complexes we have designed a family of new ligands, based on the versatile 1,2-ethanediamine moiety, with two binding pockets for manganese ions. By including or excluding carboxylate donors in the backbone of the ligands, the effects on structure and reactivity of the formed manganese complexes can be studied. Further development of these dinucleating ligands will facilitate the synthesis of complexes that better mimic the unsymmetrical and carboxylate rich environment in the active sites of MnCat and other manganese containing enzymes.

The two new ligands reported in this study, Na$_2$**L1**, and **L2** are shown in Chart 1. In Na$_2$**L1** two carboxylate groups are introduced as donor groups. The rigid non-coordinating phenylene unit in Na$_2$**L1**, and **L2** was chosen as a spacer to keep the metal centres in close proximity.

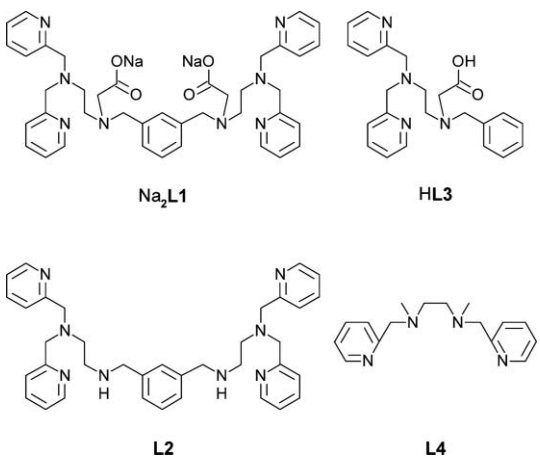

Chart 1 Ligands employed in this study.

The synthesis and characterisation of two manganese(II) complexes, [**L1**$_3$Mn(II)$_6$](ClO$_4$)$_6$ (**1**·(ClO$_4$)$_6$) and [**L2**Mn(II)$_2$(μ-OAc)(μ-Cl)](ClO$_4$)$_2$ (**2**·(ClO$_4$)$_2$), using these new ligands are also reported and their catalytic activities towards H_2O_2 disproportion are

[a]*Dept. of Photochemistry and Molecular Science, Uppsala University, P.O. Box 523, S-75120, Uppsala, Sweden. E-mail: anders.thapper@fotomol.uu.se; Fax: +46(18)4716844; Tel: +46(18)4716579*
[b]*Division of Structural Chemistry, Arrhenius Laboratory, Stockholm University, S-10691, Stockholm*

† Electronic supplementary information (ESI) available: Tables S1–S5 and Fig. S1–S11. CCDC reference numbers 746219 (**1**) and 732737 (**2**). For ESI and crystallographic data in CIF or other electronic format see DOI: 10.1039/c0dt00165a

investigated. To assess the influence of using dinucleating ligands on H_2O_2 disproportion two closely related complexes $[\mathbf{L3}Mn_4](ClO_4)_4$ ($\mathbf{3}\cdot(ClO_4)_4$)[14] and $\mathbf{L4}MnCl_2$ (**4**),[15] featuring mononucleating ligands are also studied. It is shown that, for these complexes, inclusion of the carboxylate group in the ligand (**1** and **3**) lowers the H_2O_2 disproportion activity compared to the complexes where the ligand does not contain a carboxylate group (**2** and **4**).

Results and discussion

Synthesis

The ligand $Na_2\mathbf{L1}$ was synthesised in three steps (Scheme 1) from *N*,*N*-bis(pyridin-2-ylmethyl)-ethane-1,2-diamine (**5**) which in turn was prepared from 1,2-diaminoethane according to a literature procedure.[16,17] The ligand **L2** was isolated as an intermediate in the synthesis of $Na_2\mathbf{L1}$. The mononucleating ligands H**L3** and **L4** and their corresponding manganese complexes, $\mathbf{3}\cdot(ClO_4)_4$[14] and **4**[15] were synthesised following literature procedures.

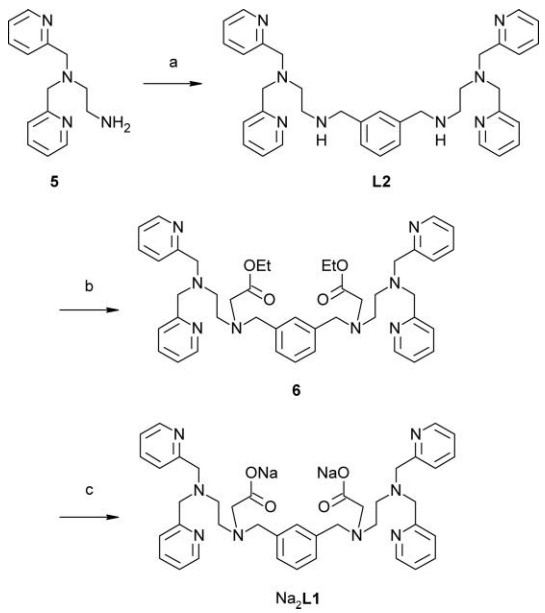

Scheme 1 Synthesis of ligands $Na_2\mathbf{L1}$ and **L2**. Reagents and conditions: (a) *1.* Isophthalaldehyde (0.5 eq.), mol. sieves, MeOH, reflux; *2.* $NaBH_4$ (3 eq), reflux (yield: 56%); (b) ethyl bromoacetate (3 eq.), Et_3N (3 eq.), CH_2Cl_2 (yield: 54%); (c) NaOH, THF : H_2O, (yield: 94%).

N,*N*-Bis(pyridin-2-ylmethyl)-ethane-1,2-diamine (**5**) was reacted with isophthalaldehyde in methanol in the presence of molecular sieves and *in situ* reduction of the imine gave the secondary amine **L2** in 56% yield. The carboxylate groups were introduced in the ligand by reacting **L2** with an excess of ethyl bromoacetate in CH_2Cl_2 to generate the ethyl di-ester (**6**), which was purified by column chromatography and isolated to give **6** in 54% yield. Finally the di-acetate ($Na_2\mathbf{L1}$) was obtained by basic hydrolysis of **6** and used for complexation without any further purification.

By dissolving manganese(II) perchlorate together with the ligand $Na_2\mathbf{L1}$ in a methanol–water mixture, a manganese(II) complex was obtained as a white solid. The isolated complex **1** was a manganese(II) hexamer instead of a dimer as intended from the ligand design. The product was recrystallised by slow diffusion of Et_2O into an acetonitrile solution of the compound to give colourless, needle-like, crystals. A reaction of **L2** with manganese(II) acetate and precipitation by addition of sodium perchlorate gave the mono-μ-acetato, mono-μ-chlorido bridged complex **2**, in low yield (<10%). The presence of a bridging chlorido ligand is tentatively explained by the *in situ* reduction of perchlorate as no other chloride source was present. This may also explain the low yield of the reaction. X-Ray quality crystals of **2** were obtained by recrystallisation from MeCN–Et_2O. The same complex could also be synthesised in higher yield (80%) using a 1 : 1 mixture of manganese(II) chloride and manganese(II) acetate as the metal source.

Crystal structures

The crystals of **1** were small and of low quality but the X-ray crystal structure could be solved and is shown in Fig. 1. The structure can be described as a dimer of manganese(II) trimers. The average Mn–Mn distance within the trimer is about 5.3 Å, and the manganese ions are bridged by a single carboxylate group to each of their neighbouring metal ions, forming 12-membered metallamacrocycles (see ESI, Fig. S1†). The two trimers are connected in the complex *via* the phenylene spacers of the ligands and the distance between the gravity points of the two trimers is 11 Å. The hexanuclear structure of complex **1** is to the best of our knowledge unique. In the crystal structure five of the six perchlorate counter ions are found surrounding the complex, while the sixth perchlorate is encapsulated inside the cavity formed by

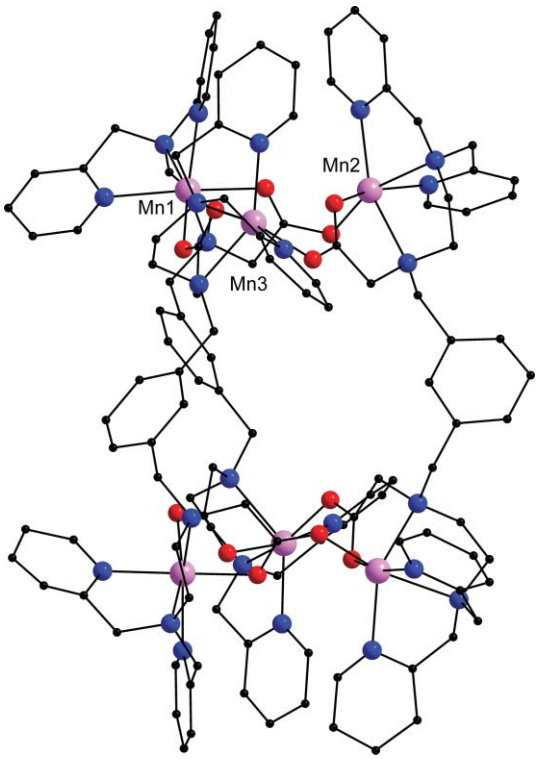

Fig. 1 Perspective view of $\mathbf{1}^{6+}$, H atoms and counter ions are omitted for clarity. Colour coding: pink = Mn; blue = N; red = O; black = C; green = Cl.

the phenylene bridges in the hexameric structure. This large cavity partly explains the low crystal density (d_c = 1.165 g cm^{-3}) observed for **1**·$(ClO_4)_6$.

The two trimers are symmetry equivalent and are close to having threefold symmetry but feature three unique manganese ions. Two of the ions, Mn1 and Mn3 are very similar in terms of bond angles around the metal whereas Mn2 deviate from the others (see ESI, Tables S1–S3†). The three manganese centres have a distorted, octahedral coordination sphere with a weak seventh bond to a carboxylate oxygen (Fig. 2). The carboxylate groups are best described as pseudo-tridentate, featuring a *syn*, *anti* $\mu_{1,3}$-ligation with a third, weak bond (shown in Fig. 2, dashed bond). Similar hepta coordination involving a $\mu_{1,3}$-ligation of a carboxylate group has been observed in two tetrameric manganese(II) complexes based on the ligands H**L3** and Hbpmg (Hbpmg = 2-((2-bis(pyridin-2-ylmethyl)amino)ethyl)(methyl)amino)acetic acid), which are mononucleating versions of Na_2**L1**.[14] A complete list of all manganese–ligand bond lengths and bond angles in **1** is found in the ESI, Tables S1–S3.† Note that due to the low quality of the crystals, the geometrical parameters should be regarded as less precise.

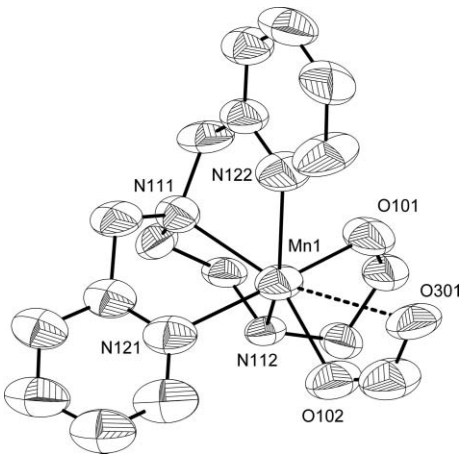

Fig. 2 Thermal ellipsoid view of one monomeric subunit in **1** (ellipsoids shown at 50% probability level), with the weak interaction between Mn1 and O301 (around 3.2 Å, dashed bond) indicated.

The crystal structure of the dimeric complex **2** is shown in Fig. 3. The two manganese centres have distorted octahedral coordination geometries. The ligand binds one metal in each binding pocket and provides four nitrogen donors to each manganese ion. The coordination sphere is completed by a $\mu_{1,3}$-acetato and a μ-chlorido bridge. The structure of **2** is to our knowledge the first example of a mono-μ-acetato, mono-μ-chlorido bridged manganese dimer. The Mn–Mn distance of 4.07 Å in **2** is intermediate between what has been found in mono-μ-chlorido- (~5 Å) and di-μ-chlorido-complexes (3.5–3.8 Å) and at the low end of what has been found for di-$\mu_{1,3}$-acetato-complexes (4.1–4.6 Å). All the manganese–ligand bonds are within the expected range for manganese(II) complexes (selected bond lengths and angles in **2** can be found in ESI, Tables S4 and S5, respectively†). It deserves mentioning that the secondary amine functionality had not been oxidised to an imine, which is clear from the N14–C25 (1.47 Å) and N24–C26 distances (1.49 Å) as well as from the residual electron density in the vicinity of N14 and N24 which matches well with the presence

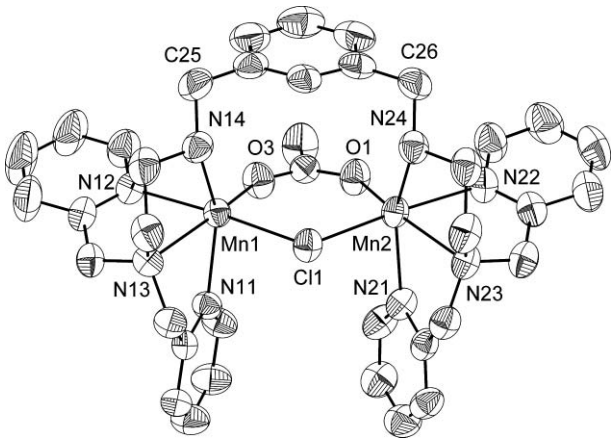

Fig. 3 Thermal ellipsoid view of **2** (ellipsoids shown at 50% probability level), H-atoms and counter ions are omitted for clarity.

of a hydrogen atom. The $\mu_{1,3}$-acetato, μ-chlorido bridging motif of complex **2**, is similar to the $\mu_{1,3}$-carboxylato, di-μ-chlorido bridging motif in the active site of chloride treated MnCat from *Thermus thermophilus*.[4]

The effect of covalently attaching the carboxylate donor to the ligand, as compared to having auxiliary carboxylate ligands present can be seen in the structures of **1** and **2**. Carboxylate groups have a tendency to adopt a bridging coordination between low valent manganese ions. In complex **2** the desired dimer is formed with the added acetate bridging two manganese ions situated in a single ligand. In complex **1** the short carboxylate arm of $\mathbf{L1}^{2-}$ prevents the formation of a bridge between two manganese ions coordinated to the same ligand. Instead each carboxylate group is bridging two manganese ions ligated to two different ligands.

Magnetic susceptibility

The molar susceptibility (χ_{mol}) of **1**·$(ClO_4)_6$ in powder form was measured in the temperature range 2–300 K under an applied magnetic field of 0.1 T. A plot of χ_{mol} and the effective magnetic moment (μ_{eff}) as a function of T for **1** is shown in Fig. 4.

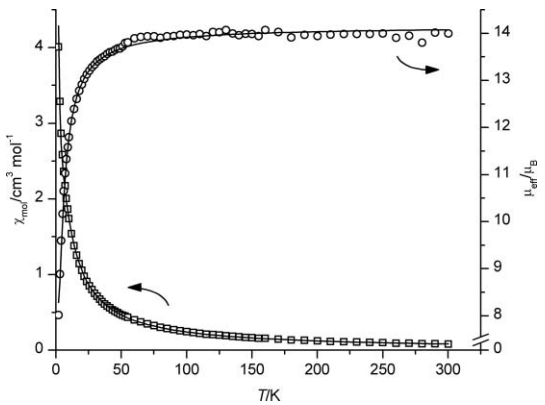

Fig. 4 Molar susceptibility, χ_{mol} (□), and effective magnetic moment, μ_{eff} (○), of **1** *vs.* temperature. Solid lines represent calculated χ_{mol} and μ_{eff} using eqn (1) and (2) with g_{eff} = 1.93 and J = –2.30 cm^{-1}.

The molar susceptibility (Fig. 4, □) continuously increased upon cooling. At higher temperatures (300–50 K) this increase was slow but accelerated below 50 K, revealing a paramagnetic ground state.

The effective magnetic moment (Fig. 4, ○) was almost constant at a value of ~14 μ_B from 300 to 50 K, where it dropped rapidly to a value of ~8 μ_B at 2 K. This indicates that antiferromagnetic interactions were present in the system.

Data analysis shows that the system can be described as two magnetically non-interacting triangular spin systems, with antiferromagnetic interaction within each ring. This model was applied when fitting the molar susceptibility and the effective magnetic moment data using eqn (1) (where $x = 3J/kT$) and eqn (2),[18]

$$\chi = \frac{Ng^2\mu_B^2}{4kT}\frac{1+5e^x}{1+e^x} \quad (1)$$

$$\mu_{eff} = \left(\frac{3\chi kT}{N\mu_B^2}\right)^{1/2} \quad (2)$$

derived from the spin Hamiltonian in eqn (3),

$$H = \sum_{\substack{i\neq j \\ i,j=1,2,3}} -2JS_iS_j \quad (3)$$

assuming an equal value for all three J couplings.

The resulting fitted curves with an effective g-value (g_{eff}) of 1.93 and $J = -2.30$ cm^{-1} are shown in Fig. 4 (solid lines).

For **1** modelled as two magnetically non-interacting triangular rings, each with three high spin manganese(II) centres ($S_T = 15/2$), the effective magnetic moment is expected to be 15.41 μ_B. The observed effective magnetic moment for **1** was 14.1 μ_B at room temperature indicating that the highest spin state $S = 15/2$ was not populated (Fig. 4).

In a triangular spin system like **1**, the antiferromagnetic interaction mode cannot be fully satisfied between each pair of spins and therefore the system experiences spin frustration. This is manifested in the molar magnetic susceptibility that shows a paramagnetic ground state in spite of the antiferromagnetic interaction within the system. The observed effective magnetic moment of 8.14 μ_B at 2 K, suggests a $S = 9/2$ ground state. Moreover, the molecular magnetisation of **1** in response to the applied field at 2 K demonstrated the spin frustration in the system (ESI, Fig. S2†).

The molar susceptibility of **2** was measured in the temperature range 2–300 K under an applied field of 0.1 T (ESI, Fig. S3†). The measurements showed antiferromagnetic interaction in the manganese(II) dimer with an exchange coupling of $J = -5.67$ cm^{-1} (see ESI for details†).

Structure of the complexes in solution

In order to elucidate if **1** and **2** retained their structures when dissolved, they were studied by a number of spectroscopic techniques and comparisons were made with spectra from powder samples.

Complex **2** is a well defined manganese(II) dimer with antiferromagnetic interaction between the manganese ions in the solid state. The EPR spectrum of **2** in a frozen MeCN solution (Fig. 5, solid line) recorded at 15 K showed features in 0–5000 G range. A set of 11 well resolved lines around 3000 G (42–45 G between two adjacent lines) was observed, typical of an EPR signal from a $Mn_2^{II,II}$ core as described by Blanchard *et al.* for a similar compound.[19]

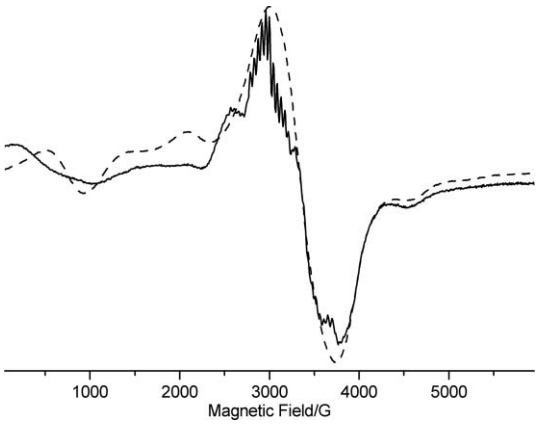

Fig. 5 EPR spectra of **2** in a KBr matrix (dashed line) and in MeCN (0.5 mM, solid line). EPR conditions: T = 15 K, microwave frequency 9.27 GHz, microwave power 20 μW; modulation frequency 100 kHz, modulation amplitude 10 G.

The weak antiferromagnetic coupling in **2** ($J = -5.67$ cm^{-1}, see magnetism section above) implies reasonable spin population of low lying excited states. Therefore the EPR spectrum is a superimposition of transitions from low lying excited states. The EPR spectrum had maximum overall intensity at 15 K.

The EPR spectrum of **2** in solid state (KBr matrix, Fig. 5 dotted line) recorded at 15 K had virtually the same spectral features in the 2500–5000 G region as the spectrum in solution, except that there were no well resolved hyperfine lines. The correspondence between frozen solution and powder EPR spectra, together with ESI-MS where the dominant peak was found to have mass 889.2 corresponding to $[\mathbf{2} - (ClO_4)^-]^+$ (calc: 889.2), shows that the dimer retains its structure in MeCN solution.

The EPR spectra of $\mathbf{1}\cdot(ClO_4)_6$ as a powder (in a KBr matrix) and in frozen solution (in MeCN) were recorded (ESI, Fig. S4†). Both spectra displayed a first derivative signal centred around g = 2 (g = 1.99 in KBr, g = 2.01 in MeCN) but no other prominent features.

A better indication of the structure of **1** in solution was obtained from comparison of frozen solution (ESI, Fig. S5–S6†) and powder form magnetic susceptibility data. The similarities in the temperature and the field dependence of **1** in frozen solution and powder form strongly supports that the hexameric structure of **1** was kept intact when the complex is dissolved in MeCN.

The solution IR spectrum (d_3-MeCN, Fig. 6, solid line) closely matched the solid state IR spectrum (KBr matrix, Fig. 6 dashed line) in the region around 1600 cm^{-1} where the asymmetric carboxylate stretch is normally observed. It is hard to identify the symmetric carboxylate stretches in the 1400–1500 cm^{-1} region but there are no indications that the coordination mode for the carboxylate groups should have changed when the complex was dissolved in MeCN.

From these spectroscopic measurements it is inferred that the two complexes, **1** and **2**, retain their structures in MeCN solution. This is important as a starting point in the following discussion of redox reactions and the H_2O_2 disproportionation activity of these complexes.

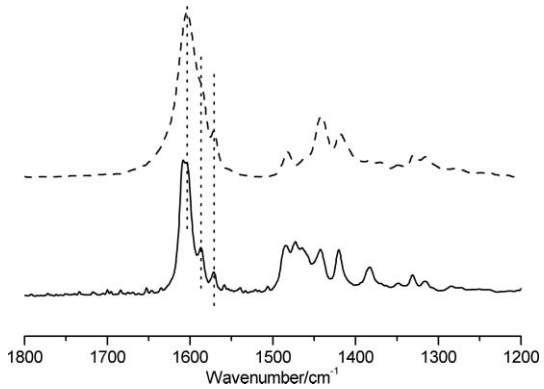

Fig. 6 IR absorbance spectra of **1** (1 mM) in d_3-MeCN with 0.1 M $TBAClO_4$ (solid line) and **1**·$(ClO_4)_6$ in solid state, ground crystals in a KBr matrix (dashed line).

Electrochemistry

The redox properties of complexes **1** and **2** were studied by both preparative and analytical electrochemical methods. The cyclic voltammetry (CV) trace of **1** in MeCN displayed three quasi-reversible redox processes, separated by approximately 300 mV each (Fig. 7(a)).[17] These redox processes, apart from a change in $\Delta E^1_{1/2}$ (*i.e.* $P^1_a - P^1_c$), did not change when the complex was oxidised up to a potential of 1.5 V (collected electrochemical data are shown in Table 1). The scan rate dependence was also examined in the range of 25–1000 mV s^{-1} and no significant changes to the CV traces were observed.

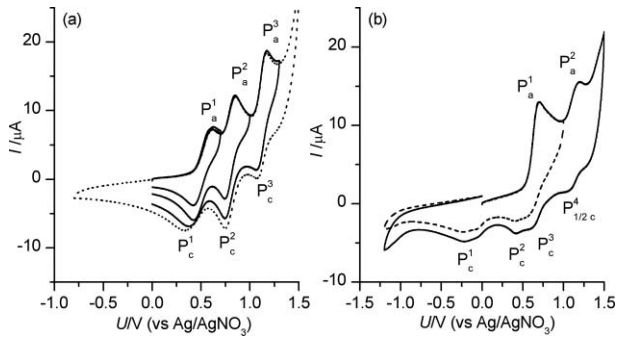

Fig. 7 The CV traces of (a) **1** (0.33 mM) and (b) **2** (0.5 mM) in MeCN, with 0.1 M $TBAClO_4$ as supporting electrolyte, scan rate 0.1 V s^{-1}, 20 °C. Peaks are labelled with P_a for anodic peaks and P_c for cathodic peaks. $P_{1/2}$ is used when no clear peak is discernible.

Table 1 Electrochemical data for **1** and **2** (in V). The $E_{1/2}$ $((P_a + P_c)/2)$ for the redox couples for **1** ($\Delta E_p = P_a - P_c$ in parenthesis), and the anodic (P_a) and cathodic (P_c) potentials at the peak currents for **2**. $P_{1/2}$ is the potential at half peak-height where no clear peak was discernible

1	2
$E^1_{1/2} = +0.50$ (0.24)	$P^1_a = +0.71$
$E^2_{1/2} = +0.80$ (0.09)	$P^2_a = +1.19$
$E^3_{1/2} = +1.11$ (0.06)	$P^1_c = -0.22$
	$P^2_c = +0.42$
	$P^3_c = +0.59$
	$P^4_{1/2c} = +1.1$

Potentials are given *vs.* $Ag/AgNO_3$ $[AgNO_3] = 0.010$ M.

In contrast, the CV trace of complex **2** displayed irreversible redox chemistry (Fig. 7(b)). Scanning up to a potential of 1 V, one anodic and three cathodic processes were observed (Fig. 7(b), dotted line, Table 1). If the cathodic scan was reversed at 0.1 V the oxidation process was not fully reversible, and the intensity of the anodic peak dropped upon multiple scans (ESI, Fig. S7†). When scanning up to 1.5 V a second redox couple appeared (Fig. 7(b), solid line, Table 1). The appearance of multiple reduction processes during the cathodic scan and the large shifts between the anodic and cathodic waves show that chemical reactions occurred in connection to the electrochemical redox processes.

In order to determine the nature of the redox processes for both **1** and **2**, preparative electrochemistry at controlled potentials was employed and the obtained oxidised products were analysed by EPR spectroscopy.

Exhaustive bulk electrolysis of a solution of **1**·$(ClO_4)_6$ at 0.7 V consumed two equivalents of electrons per hexamer, and an EPR spectrum recorded at 20 K of the resulting orange solution showed complete disappearance of the starting signal from **1** while a new signal with a low field feature at $g \sim 6$, and a $g = 2$ part appeared (ESI, Fig. S8B†). Continued oxidation at 0.9 V consumed another two equivalents of electrons per hexamer, and resulted in further changes in the low field region of the EPR spectrum together with the appearance of a weak 510 G wide six-line signal centred around $g = 2$ (ESI, Fig. S8C†). Finally, electrolysis at 1.45 V consumed two more equivalents of electrons per hexamer, at this point the six-line signal in the EPR spectrum had increased five-fold in intensity (ESI, Fig. S8D†).

Based on the coulometry observed during bulk electrolysis and the reversibility of the electrochemical reactions, the three redox processes are assigned as arising from $Mn^{(III/II)}$ redox processes occurring simultaneously in the two trimeric subunits. Consequently bulk electrolysis at 0.7 V results in a $(Mn_3^{II,II,III})_2$ complex and the species obtained after bulk electrolysis at 0.9 V and 1.45 V are assigned to a $(Mn_3^{II,III,III})_2$ species and a $(Mn_3^{III,III,III})_2$ species respectively. The six-line EPR signal appearing following oxidation at high oxidising potential is a fingerprint signal of monomeric manganese(II) ions, this is attributed to partial degradation of the material as a result of the extended bulk electrolysis.

Subjecting complex **2** to exhaustive bulk electrolysis at 0.95 V consumed one equivalent of electrons per manganese ion. The EPR spectrum of the oxidised red solution (ESI, Fig. S9B†) showed no EPR signal from **2**. Thus most of the manganese ions were present in an EPR silent spin state, either as a mononuclear manganese(III) species or as a $Mn_2^{III,III}$ dimer. A small (< 10%) 16-line EPR signal from a di-μ-oxo $Mn_2^{III,IV}$ dimer[20] was observed. Continued bulk electrolysis at 0.95 V consumed another 0.5 equivalents of electrons per manganese ion. The corresponding EPR spectrum at this point showed an eight-fold increase in the di-μ-oxo $Mn_2^{III,IV}$ species,[20] and a six-line EPR signal attributed to a monomeric manganese(II) species (ESI, Fig. S9C–D†).

Based on the combined data from analytical and preparative electrochemistry, the two oxidation waves in the CV of **2** are assigned to manganese based oxidations. The first oxidation is a $Mn_2^{II,II}$ to $Mn_2^{III,III}$ oxidation, supported by the experiment combining coulometry and EPR.[21] The second oxidation in the CV trace of **2** is connected with a manganese(III) to manganese(IV) oxidation, as an increase in the $Mn_2^{III,IV}$ EPR signal intensity could be observed after further bulk electrolysis. The complex behaviour

on the reverse scan is attributed to the chemical reactions expected upon oxidation of this type of complex,[23,24] which result in a mixture of species. The width of the 16-line EPR spectrum (1230 G) suggests that the original bridging acetate and chloride ligands are replaced by aqua derived ligands upon oxidation, which in turn stabilises the higher charge of the complex by deprotonation to form two μ-oxo bridges. The oxidised complex is not stable and the degradation, observed with EPR spectroscopy, upon extended electrolysis is attributed to the release of protons during the formation of the oxo-bridges, forcing the ligand to act as base, as has been reported for similar systems.[20,25]

To summarise the observations from the electrochemical study it is apparent that the stability of it between the manganese ions is dependent on if the bridging moiety is an external ligand or a part of the ligand backbone. Complex **2** showed ligand rearrangement already after the first oxidation process as shown by the multiple reduction processes in the CV and the formation of two μ-oxo bridges when the complex was oxidised to the $Mn_2^{III,IV}$ state. Chemical reactions are known to be coupled to the electrochemical event for manganese complexes with labile ligands, *e.g.* acetates.[24,26] Complex **1** on the other hand could be oxidised several steps without ligand rearrangement. The macrocyclic structure was retained at higher oxidation states preventing coordination of aqua ligands and as a consequence no higher oxidation state than manganese(III) could be reached.

Hydrogen peroxide disproportionation studies

To evaluate the difference between complexes **1–4** in their capacity to perform catalase-like chemistry (*i.e.* the disproportionation of H_2O_2 into H_2O and O_2), the complexes were treated with H_2O_2 in a Clark-type electrochemical cell. The initial rates (V_{max}) of the disproportionation reactions were estimated from the O_2 evolution (V_{max}). In a typical experiment, acetonitrile solutions of the complexes ([Mn] = 0.02–1.6 mM) were equilibrated to air before a large excess of H_2O_2 was added. Typical O_2-traces are shown in Fig. 8. Lag phases of about 60 s and 30 s were present for **1** and **3** respectively whereas the O_2 evolution starts almost immediately for complex **2** and **4** (the initial small dip in the oxygen concentration is a solvent mixing effect when the H_2O_2(aq) is added to the MeCN solution of the complex). The V_{max} for **2** and **4** are about three orders of magnitude higher than for **1** and two orders of magnitude higher than for **3** (Table 2).[27]

By varying the concentration of the complexes ([Mn] = 0.4–1.6 mM (**1**), 0.02–0.20 mM (**2**), 0.1–0.4 mM (**3**) and 0.03–0.10 mM (**4**)) the disproportionation of H_2O_2 was found to follow pseudo-first-order kinetics for all four complexes (see ESI, Fig. S10†).

The reactions were also monitored by EPR spectroscopy, by performing a separate set of experiments where the complexes ([Mn] = 0.5 mM) were treated as described above, 100 μL aliquots were taken at set times (15 s, 60 s, and 3 min) and freeze quenched in liquid nitrogen prior to EPR measurements. For

Table 2 Maximum rates of oxygen evolution (V_{max}) in mol $O_2 \cdot s^{-1}$ mol Mn^{-1} for complexes **1–4** ([Mn] = 0.4–1.6 mM (**1**), 0.02–0.20 mM (**2**), 0.1–0.4 mM (**3**) and 0.03–0.10 mM (**4**) treated with 2.3 M H_2O_2

Complex	**1**	**2**	**3**	**4**
V_{max}	$4.1 \pm 0.2 \times 10^{-3}$	1.74 ± 0.02	$31 \pm 3 \times 10^{-3}$	4.18 ± 0.07

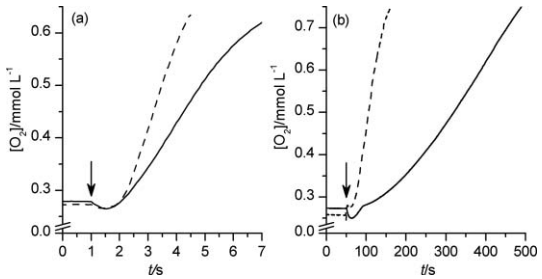

Fig. 8 Oxygen evolution traces from H_2O_2 disproportionation by (a) **2** (0.03 mM, solid line) and **4** (0.06 mM, dashed line), and (b) **1** (0.083 mM, solid line) and **3** (0.05 mM, dashed line) in MeCN. The arrows indicate injection of H_2O_2 (2.3 M) to air saturated solutions. Notice the different time scales in (a) and (b). $TBAPF_6$ (0.1 M) was present in all solutions. $T = 20$ °C.

complex **1** the starting manganese(II) EPR signature did not change to any great extent after addition of H_2O_2 and no other signals were detectable in the spectra throughout the experiment (ESI, Fig. S11a†). Complex **3** showed a starting EPR signal almost identical to that of **1** (ESI, Fig. S11c†). After addition of H_2O_2 the EPR signal changed, the $g = 2$ feature decreased and additional low field features at $g \sim 3.5$ and $g \sim 5.5$ appeared (ESI, Fig. S11c†). This new signal closely resembles the EPR signal from $[(mgbpen)_2Mn_2^{II,II}(H_2O)_2]^{2+}$ (Hmgbpen = *N*-methyl-*N*′-glycyl-*N*,*N*′-bis(2-pyridylmethyl)ethane-1,2-diamine),[8] a co-ordinately saturated manganese(II) dimer with $\mu_{1,1}$-carboxylate bridges. We conclude that the complex stays in a manganese(II) state but that the tetrameric structure of **3** has been altered. During the three minutes after addition of H_2O_2 the complex remained in this manganese(II) state. In MS no traces of higher oxidation state oxo bridged manganese species could be detected. In an experiment where H_2O_2 was added directly to solutions of **3** ([Mn] = 0.5 mM) in EPR-tubes an almost complete conversion to the new manganese(II) state was observed directly (1–2 s) after addition *i.e.* well before oxygen evolution was observed in the Clark experiment.

For complexes **2** and **4** the situation was very different and 15 s after addition of H_2O_2 more than 50% of the manganese atoms were present as a di-μ-oxo $Mn_2^{III,IV}$ species (ESI, Fig. S11b and S11d,† see experimental for details on the quantification). The $Mn_2^{III,IV}$ EPR signal remained during the three minutes that the reactions were followed together with a small 6-line EPR signal from solvated manganese(II). In a separate set of experiments H_2O_2 was added directly to solutions of **2** ([Mn] = 0.5 mM) in EPR tubes. Quantification of the $Mn_2^{III,IV}$ EPR signal in these samples showed that 1–2 s after addition of H_2O_2 more than 40% of the manganese ions had formed a di-μ-oxo $Mn_2^{III,IV}$ species. No traces of radical species could be detected by EPR in any of the experiments.

These observations lead to the following conclusions about the reaction mechanism for H_2O_2 disproportionation by the four complexes:

The immediate O_2 evolution for complexes **2** and **4**, together with the high V_{max}, is attributed to that the structure in solution contains open coordination sites, easily accessible for the substrate. This is in line with that the small auxiliary ligands (acetate and chloride) are easily displaced as was observed for **2** in the electrochemical study.

The longer lag phase and lower rate of O_2 evolution observed for complexes **1** and **3** are interpreted as a requirement for larger structural rearrangement, *e.g.* an opening of the metallamacrocyclic structure of these complexes to turn into the active catalysts. The chelate effect makes dissociation of any of the ligands more difficult and therefore no coordination site is available for the substrate. This is in line with the idea that **1** (initially) retains its dimer of trimers type of structure in solution.[28] A similar argument can be made for the manganese(II) species formed upon addition of H_2O_2 to **3**.

Additionally, different reaction mechanisms should lie behind the differences in redox behaviour observed upon treatment with H_2O_2. For complexes **1** and **3** the dominant manganese(II) EPR signals after H_2O_2 addition suggest a mechanism involving manganese(II) and manganese(III) oxidation states, as observed for the natural enzyme,[29] with the rate determining step being the oxidation of manganese(II) to manganese(III). For complexes **2** and **4** a distinctly different mechanism appears to be responsible for the activity where most of the manganese is present as a $Mn_2^{III,IV}$ species, suggesting the involvement of higher oxidation states in the mechanism. Such a mechanism, cycling between $Mn_2^{II,III}$ and $Mn_2^{III,IV}$ has recently been suggested by Lessa *et al.* for a dinuclear Mn-complex based on the HPCINOL ligand (HPCINOL = 1-(bis pyridine-2-ylmethyl-amino)-3-chloropropan-2-ol),[30] and Dubois *et al.* for a series of more closely related ligands based on tpa (tpa = tris(pyridin-2-ylmethyl)amine) and derivatives thereof.[6] The tendency for **1** and **3** to stay in lower oxidation states could be attributed to the higher denticities of Na_2**L1** and H**L3** respectively, suppressing the formation of high-valent Mn-complexes by preventing the formation of a di-μ-oxo core.

Conclusion

In this article the synthesis and characterisation of two ligands and their manganese complexes, **1** and **2**, both featuring novel structural motifs, have been described. In addition the ability of the complexes to perform catalase-like disproportionation of hydrogen peroxide has been investigated.

The X-ray crystal structures obtained show that supplying the carboxylate donor as a part of the ligand backbone instead of having it as an auxiliary ligand greatly shifts the coordination behaviour. Ligand **L2** yielded a dinuclear structure featuring a μ-acetato, μ-chlorido bridging motif. In contrast, the geometry enforced by **L1**$^{2-}$, where carboxylates are part of the ligand backbone, prevented the carboxylates from acting as bridging ligands between two manganese ions in the same ligand. Instead of a dinuclear structure this resulted in an unexpected hexameric structure with Mn–Mn distances of over 10 Å for two manganese ions bound to the same ligand.

In order to evaluate the nature of the complexes in solution, EPR, IR, and mass spectroscopy, analytic electrochemistry and magnetic susceptibility were used. While EPR spectroscopy was sufficient to conclude that complex **2** stayed intact in solution, a combination of IR spectroscopy and magnetic susceptibility was used to verify that the hexameric structure of **1** was retained in solution.

The H_2O_2 disproportionation study showed that the complex structures imposed by **L1**$^{2-}$ and **L3**$^{-}$ led to significantly lowered reactivities of the manganese complexes **1** and **3** respectively compared to those of **2** and **4**. As **2** shows similar turnover rate as **4** and the turnover rates of **1** and **3** are not dramatically different, the geometry imposed by the dinucleating ligands is not the major cause of the large rate difference between the complexes. The decrease in rate can instead be attributed to the higher denticity of the ligands in complex **1** and **3** that will lower the substrate access and prevent a reaction mechanism involving high-valent intermediates.

To conclude, the structure and reactivity of complex **2** show that this type of dinucleating ligand framework is a promising candidate for further development of asymmetric ligands, leading to complexes that better mimic the active site of MnCat and other redox active metalloenzymes. The ligand design has to provide a well defined ligand environment while still allowing for the flexibility needed for efficient catalysis (*e.g.* in terms of available coordination sites for substrate).

Experimental

General remarks

Dichloromethane, methanol, tetrahydrofuran and diethyl ether were distilled under appropriate drying agents.[31] Column chromatography was performed using alumina gel (activated, neutral, 150 mesh, deactivated with 4% H_2O). All other reagents were of reagent grade and used as received. NMR spectra were recorded on a JEOL 400 MHz spectrometer. NMR chemical shifts are reported in ppm relative to the solvent peak. *J*-values are given in Hz. ESI-MS was recorded on a Finnigan LCQ Deca XP MAX unless otherwise stated. IR spectra were recorded on a Bruker IFS 66v/S spectrometer and the samples were ground in a KBr matrix or dissolved in analytical grade d_3-MeCN. Elemental analysis (C, H, N, Mn) was performed by Analytische Laboratorien GmbH, Lindlar, Germany.

Caution: Perchlorate salts are potentially explosive and should be handled with care.

Synthesis

N,*N*-Bis(pyridin-2-ylmethyl)-ethane-1,2-diamine (**5**),[16,17] [**L3**-Mn_4]$(ClO_4)_4$, (**3**)[14] and **L4**$MnCl_2$ (**4**)[15] were synthesised in accordance with literature procedures.

***N1*,*N1′*-(1,3-phenylenebis(methylene))bis(*N2*,*N2′*-bis(pyridin-2-ylmethyl)ethane-1,2-diamine), L2.** Isophthaldehyde (141 mg, 1.42 mmol) was mixed with the amine, **5** (690 mg, 2.85 mmol) in MeOH (15 mL) and mol. sieves (4 Å). The reaction mixture was refluxed for 24 h under N_2, cooled to ambient temperature and an excess of $NaBH_4$ (3 eq.) was added. When the vigorous reaction had subsided the solution was taken to reflux for 3 h. At the end of the reaction H_2O (20 mL) was added and the solution was concentrated under reduced pressure, followed by filtration. The filter-cake was washed with CH_2Cl_2 and the organic phase separated. The aqueous layer was extracted with CH_2Cl_2 (3 × 25 mL). The combined organic fractions were dried using anhydrous Na_2SO_4, filtered and finally concentrated *in vacuo* to give the product as a yellow oil. Yield: 467 mg (56%). NMR ^{1}H ($CDCl_3$, 400 MHz), δ (ppm): 8.50 4H (ddd, J = 4.9, 1.7, 0.8); 7.63 4H (ddd, J = 7.7, 7.4, 1.7); 7.45 4H (ddd, J = 7.7, 0.9, 0.8); 7.33–7.21 4H (m); 7.14 (ddd, J = 7.4, 4.9, 0.9); 3.86 8H (s); 3.73

4H (s); 2.87–2.76 8H (m); ^{13}C ($CDCl_3$, 100 MHz), δ (ppm): 159.1; 148.6; 139.4; 136.2; 128.2; 127.8; 126.6; 122.7; 121.7; 60.2; 53.5; 53.1; 46.2. ESI-MS: (m/z) 587.5 $[M + H^+]^+$ (calc: 587.4).

Diethyl 2,2′-(1,3-phenylenebis(methylene))bis((2-(bis(pyridin-2-ylmethyl)amino)ethyl)azanediyl)diacetate, 6. The amine, **L2** (422 mg, 0.72 mmol) was dissolved in CH_2Cl_2 and cooled to 0 °C before ethyl bromoacetate (355 mg, 2.13 mmol) and Et_3N (218 mg, 2.15 mmol) was added. The reaction mixture was slowly heated to ambient temperature and stirred over night. The solution was basified by addition of sat. aqueous K_2CO_3 (20 mL) and the resulting mixture was extracted with CH_2Cl_2 (3 × 25 mL). The combined organic phases were dried using Na_2SO_4, filtered and the solution concentrated *in vacuo* to give the crude product as a brown oil. The material was purified by column chromatography, eluting with CH_2Cl_2 : MeOH 98 : 2 to give the product as a brownish oil. Yield: 293 mg (54%). NMR ^{1}H ($CDCl_3$, 400 MHz), δ (ppm): 8.45 4H (ddd, J = 4.9, 1.8, 0.8); 7.56 4H (ddd J = 7.8, 7.4, 1.8); 7.45 4H (ddd, J = 7.8, 1.1, 0.8); 7.13–7.08 4H (m); 7.07 4H (ddd, J = 7.4, 4.9, 1.1); 4.04 4H (q, J = 7.1); 3.75 8H (s); 3.63 4H (s); 3.19 4H (s); 2.84–2.76 4H (m) 2.69–2.61 4H (m); 1.16 6H (t, J = 7.1); ^{13}C ($CDCl_3$, 100 MHz), δ (ppm): 171.4; 159.8; 148.9; 138.8; 136.4; 129.4; 128.2; 127.7; 122.9; 121.9; 60.6; 60.1; 58.4; 54.3; 52.4; 51.5; 14.3. ESI-MS: (m/z) 759.45 $[M + H^+]^+$ (calc: 759.4).

Sodium 2,2′-(1,3-Phenylenebis(methylene))bis((2-(bis(pyridin-2-ylmethyl)amino)ethyl)azanediyl)diacetate, Na_2L1. The ester, **6**, was hydrolyzed by stirring it in a mixture of THF (3 mL) and water (4 mL) and a few drops of NaOH (2 M) for 36 h. The reaction mixture was then washed using CH_2Cl_2 and the resulting organic phase extracted twice with weakly basic H_2O. The combined aqueous phases were evaporated under reduced pressure and the resulting solids were extracted into CH_2Cl_2, the yellow solution was filtered and evaporated to give the product as beige solids. Yield: 877 mg (94%) NMR ^{1}H (CD_3OD, 400 MHz), δ (ppm): 8.79 4H (ddd, J = 5.6, 1.5, 0.7); 8.34 4H (ddd, J = 7.9, 7.6, 1.5); 7.92 1H (d, J = 1.5); 7.90 4H (dm, J = 7.9); 7.82 4H (ddd = 7.6, 5.6, 0.8); 7.68 2H (dd, J = 7.7, 1.5); 7.53 1H (t, J = 7.7); 4.54 4H (s); 4.33 8H (s); 4.06 4H (s); 3.66 4H (t, J = 6.3); 3.33 4H (t, J = 6.3); ^{13}C (CD_3OD, 100 MHz), δ (ppm): 169.7; 154.9; 145.7; 145.3; 136.5; 134.7; 131.9; 131.3; 127.8; 126.9; 59.3; 57.7; 54.1; 52.6; 51.2. ESI-MS: (m/z) 703.45 $[M - 2\ Na^+ + 3\ H^+]^+$ (calc: 703.4).

$L1_3Mn_6(ClO_4)_6$, 1·$(ClO_4)_6$. The ligand (Na_2**L1**) (358 mg, 0.5 mmol) was dissolved in a de-aerated 1 : 1 mixture of MeOH and H_2O (30 mL) and heated to 50 °C before a solution of $Mn(ClO_4)_2{\cdot}6H_2O$ (370 mg, 1.0 mmol) in MeOH (5 mL) was added dropwise. The reaction mixture was left without stirring under N_2 while the temperature was slowly lowered to ambient temperature (4 days). The white solids that appeared were filtered off and washed with water and Et_2O. X-Ray quality crystals were obtained by slow diffusion of Et_2O into a MeCN solution of the complex. Yield: 300 mg (68.8%). $C_{120}H_{132}Cl_6Mn_6N_{24}O_{36}$ (3028.8). Calc (**L1**$_3Mn_6(ClO_4)_6{\cdot}2H_2O$): C, 45.95; H, 4.63; N, 10.72; Mn, 10.51; found: C, 45.83; H, 4.64; N, 10.63; Mn, 10.36. ESI-MS: (m/z) 909.2 $[1/3\ M - (ClO_4)^-]^+$ (calc: 909.2).

$[L2Mn_2(\mu_{1,3}\text{-}OAc)(\mu\text{-}Cl)](ClO_4)_2$, 2·$(ClO_4)_2$. The secondary amine **L2** (313 mg, 0.53 mmol) was dissolved in MeOH (20 mL) before $Mn(OAc)_2$ (280 mg, 1.1 mmol) was added. The weakly brown reaction mixture was stirred for 45 min before $NaClO_4$ (305 mg, 2.5 mmol) dissolved in H_2O (1.5 mL) was added. After 7 days at –20 °C the complex had precipitated as maroon coloured crystals. The solids were filtered off and washed with H_2O and Et_2O before being recrystallised by vapour diffusion of Et_2O into a concentrated acetonitrile solution. Yield: 50 mg (9.6%). Alternatively $MnCl_2$ (113 mg, 0.9 mmol) and $Mn(OAc)_2$ (221 mg, 0.9 mmol) was added to an argon flushed solution of **L2** (96 mg, 0.16 mmol) dissolved in MeOH (7 mL). The reaction mixture was stirred for 2 h at room temperature under a nitrogen atmosphere. $NaClO_4$ (470 mg, 3.8 mmol) dissolved in 0.7 mL H_2O was added to the solution that was kept stirring for 6 h and then placed at –20 °C for 2 days. The product was obtained as a beige solid. Yield 130 mg (80%). $C_{38}H_{45}Cl_3Mn_2N_8O_{10}$ (990.0) calc.: C 46.10; H 4.58; N, 11.32; Mn, 11.10; found: C 46.06; H 4.64; N 11.22; Mn 11.07. ESI-MS: (m/z) 889.2 $[M - (ClO_4)^-]^+$ (calc: 889.2).

Hydrogen peroxide disproportionation studies

The rate constants of the catalase-like reactions were determined using a standard Clark-type oxygraph electrode (Hansatech Instruments), separated from the sample solution by a Teflon membrane. The signal was recorded for the entire duration of the experiment at 0.1 s intervals using the Oxygraph+ software (Hansatech Instruments), the same software was used for determination of the rates at the steepest slope of the reaction. The signal was calibrated using air saturated aqueous solutions ($[O_2]$ = 276 μM, T = 20 °C). In a standard procedure, the desired amount of catalyst was dissolved in acetonitrile, 1 mL, containing 0.1 M tetrabutylammonium hexafluorophosphate ($TBAPF_6$) to give concentrations ranging 0.02 mM to 1.6 mM, H_2O_2 (250 μL, 2.9 mmol) was added from a stock solution in H_2O.

Electrochemistry

Cyclic voltammetry and controlled potential electrolysis were carried out by using an Autolab potentiostat with a GPES electrochemical interface (Eco Chemie). Sample solutions (4 mL) were prepared from dry acetonitrile containing 0.1 M $TBAClO_4$ (Fluka, electrochemical grade) as supporting electrolyte. For cyclic voltammetry, the working electrode was a glassy carbon disc (diameter 3 mm). All cyclic voltammograms shown were recorded at a scan rate of 0.1 V s^{-1}. A glassy carbon rod served as counter electrode, and the reference electrode was an Ag/Ag^+ electrode (a silver wire immersed into 10 mM $AgNO_3$ in MeCN) with a potential of –0.07 V *vs.* the ferrocene/ferrocenium (Fc/Fc^+) couple in dry MeCN. Counter and reference electrode were in compartments separated from the bulk solution by fritted disks and were the same for all analytical and bulk electrochemical experiments. Before all measurements, oxygen was removed by bubbling solvent-saturated argon through the stirred solutions. Samples were kept under argon during measurements. To obtain EPR spectra of the complexes in different oxidation states, solutions prepared in the same way as described above for analytical electrochemistry were subjected to bulk electrolysis at controlled potentials. A cylindrical platinum grid (*ca.* 4 cm^2) was used as working electrode for bulk electrolysis. The electrolysis was monitored by amperometry and coulometry and took 3–5 min to completion. After electrolysis, samples of 100 μL were taken from

the solution, with an air-tight, argon-filled syringe, transferred to argon-flushed EPR tubes, frozen and stored in liquid nitrogen.

X-Ray crystallography†

Crystal data for **1**: $[(C_{40}H_{44}N_8O_4)Mn_2]_3(ClO_4)_6$, ($C_{120}H_{132}Cl_6Mn_6N_{24}O_{36}$), white needles, Fw = 3028.84, tetragonal, space group $P4_2/n$, $a = 26.7119(3)$ Å, $c = 24.2013(5)$ Å, $V = 17268.2(5)$ Å^3, $d_c = 1.165$ g cm^{-3}, $Z = 4$, $T = 100(2)$ K, $\mu(\lambda = 0.90769\ \text{Å}) = 1.140$ mm^{-1}, $R_{int} = 0.0542$, $N_{measured} = 29\,388$, $N_{unique} = 13\,671$, w$R_2 = 0.4092$ (all 13 671 data) and $R_1 = 0.1532$ (7708 data with $I \geq 2\ \sigma(I)$).

The diffraction data were collected on beam-line I911-5 at the Swedish synchrotron facility MaxLab, Lund. The data was obtained with a MARCCD 165 detector using ϕ-scans.

Due to the large amount of solvent accessible voids (approximately 5400 Å^3) in the structure of (**1**·$(ClO_4)_6$) the data were subjected to the SQUEEZE procedure available in PLATON to remove contributions to the diffraction data from disordered solvent. One of the perchlorate ions was modelled as disordered over two positions. The structure analysis was done with direct methods using SHELXD[32] and refined with full-matrix least-square calculations using SHELXH97.[32] Anomalous dispersion correction terms for the used wavelength (0.9083 Å) obtained from WCROMER.[33,34]

Crystal data for **2**: $[(C_{36}H_{42}N_8)Mn_2(C_2H_3O_2)Cl]$ $(ClO_4)_2$, ($C_{38}H_{45}Cl_3Mn_2N_8O_{10}$), colourless plates, Fw = 990.05, monoclinic, space group $C2/c$, $a = 19.2617(9)$ Å, $b = 14.0395(7)$ Å, $c = 36.5344(16)$ Å, $\beta = 93.564(4)°$, $V = 9860.7(8)$ Å^3, $d = 1.334$ g cm^{-3}, $Z = 8$, $T = 293(2)$ K, μ(Mo-Kα) = 0.732 mm^{-1}, $R_{int} = 0.0694$, $N_{measured} = 59\,669$, $N_{unique} = 10\,048$, w$R_2 = 0.1640$ (all 10048 data) and $R_1 = 0.0482$ (5617 data with $I \geq 2\ \sigma(I)$).

The diffraction data was collected on an Excalibur-II κ diffractometer equipped with a sapphire-III CCD detector, both from Oxford Diffraction. The structure analysis was done with direct methods using SHELXS97[32] and refined with full-matrix least-square calculations using SHELXL97.[32]

EPR spectroscopy

EPR spectra were recorded at X-band range using Bruker ELEXSYS-E500 spectrometer equipped with an ER0601SHQE resonator or a DM9807 resonator. Liquid helium temperature controller Oxford ITC503 and ESR900 cryostat were used for temperature control. Quantification of $Mn_2^{III,IV}$ EPR signals were made by double integration of the signals recorded at 20 K using a microwave power of 20 μW. The size of the signal was compared to the size of the doubly integrated $Mn_2^{III,IV}$ EPR signal of $[Mn_2(\mu\text{-}O)_2(H_2O)_2(tpy)_2]^{3+}$ (1 mM)[35] measured under the same conditions. This quantification gives an approximate accuracy of ±5%.

Magnetic susceptibility

Magnetic susceptibilities of **1** and **2** were measured on a Quantum Design MPMS SQUID susceptometer equipped with a superconducting magnet operating in ±7 T and a continuous temperature controller operating in 1.9–400 K range. Samples of **1** and **2** were kept in a sample bucket with lid. Data were recorded using RSO (reciprocating sample option) detecting mode and background subtraction option. No further corrections were made in the data analysis. Temperature dependence of mol susceptibility of **1** and **2** were measured at a fixed field of 1 kOe, and field dependence of molar longitudinal moment was measured at 2 K.

Acknowledgements

This work was supported by grants from the Swedish Energy Agency, Knut and Alice Wallenberg Foundation and the EU/Energy Network project SOLAR-H2 (FP7 contract no. 212508).

Notes and references

1 N. A. Law, M. T. Caudle and V. L. Pecoraro, in *Adv. Inorg. Chem.*, ed. A. G. Sykes, Academic Press, 1998, vol. 46, pp. 305–440.
2 B. Halliwell and J. M. C. Gutteridge, in *Methods Enzymol.*, ed. L. Packer and A. N. Glazer, Academic Press, 1990, vol. 186, pp. 1–85.
3 E. R. Stadtman, B. S. Berlett and P. B. Chock, *Proc. Natl. Acad. Sci. U. S. A.*, 1990, **87**, 384–388.
4 S. V. Antonyuk, V. R. Melik-Adamyan, A. N. Popov, V. S. Lamzin, P. D. Hempstead, P. M. Harrison, P. J. Artymyuk and V. V. Barynin, *Crystallogr. Rep.*, 2000, **45**, 105–116.
5 V. V. Barynin, M. M. Whittaker, S. V. Antonyuk, V. S. Lamzin, P. M. Harrison, P. J. Artymiuk and J. W. Whittaker, *Structure*, 2001, **9**, 725–738.
6 L. Dubois, J. Pécaut, M.-F. Charlot, C. Baffert, M.-N. Collomb, A. Deronzier and J.-M. Latour, *Chem.–Eur. J.*, 2008, **14**, 3013–3025.
7 S.-Y. Liu, J. D. Soper, J. Y. Yang, E. V. Rybak-Akimova and D. G. Nocera, *Inorg. Chem.*, 2006, **45**, 7572–7574.
8 C. Baffert, M. N. Collomb, A. Deronzier, S. Kjærgaard-Knudsen, J. M. Latour, K. H. Lund, C. J. McKenzie, M. Mortensen, L. P. Nielsen and N. Thorup, *Dalton Trans.*, 2003, 1765–1772.
9 X. Jiang, H. Liu, B. Zheng and J. Zhang, *Dalton Trans.*, 2009, 8714–8723.
10 A. J. Wu, J. E. Penner-Hahn and V. L. Pecoraro, *Chem. Rev.*, 2004, **104**, 903–938.
11 L. Dubois, D.-F. Xiang, X.-S. Tan, J. Pécaut, P. Jones, S. Baudron, L. Le Pape, J.-M. Latour, C. Baffert, S. Chardon-Noblat, M.-N. Collomb and A. Deronzier, *Inorg. Chem.*, 2003, **42**, 750–760.
12 B.-H. Ye, T. Mak, I. D. Williams and X.-y. Li, *Chem. Commun.*, 1997, 1813–1814.
13 S.-B. Yu, S. J. Lippard, I. Shweky and A. Bino, *Inorg. Chem.*, 1992, **31**, 3502–3504.
14 G. Berggren, A. Thapper, P. Huang, P. Kurz, L. Eriksson, S. Styring and M. F. Anderlund, *Dalton Trans.*, 2009, 10044.
15 C. Hureau, G. Blondin, M.-F. Charlot, C. Philouze, M. Nierlich, M. Césario and E. Anxolabéhère-Mallart, *Inorg. Chem.*, 2005, **44**, 3669–3683.
16 E. Kawabata, K. Kikuchi, Y. Urano, H. Kojima, A. Odani and T. Nagano, *J. Am. Chem. Soc.*, 2005, **127**, 818–819.
17 K.-Q. Ling and L. M. Sayre, *J. Am. Chem. Soc.*, 2005, **127**, 4777–4784.
18 C. J. O'Connor, *Prog. Inorg. Chem.*, 1982, **29**, 203–283.
19 S. Blanchard, G. Blondin, E. Rivière, M. Nierlich and J.-J. Girerd, *Inorg. Chem.*, 2003, **42**, 4568–4578.
20 C. Hureau, L. Sabater, E. Anxolabéhère-Mallart, M. Nierlich, M.-F. Charlot, F. Gonnet, E. Rivière and G. Blondin, *Chem.–Eur. J.*, 2004, **10**, 1998–2010.
21 It should be noted that chloride oxidation has been observed in a manganese(II) chloride complex at about the same potential as the first oxidation of **2**.[22] We cannot distinguish direct oxidation of a manganese ion from the case where a chloride bridge in **2** is oxidised and the then formed radical proceeds to oxidise manganese.
22 G. Berggren, P. Huang, L. Eriksson and M. F. Anderlund, *Appl. Magn. Reson.*, 2009, **36**, 9–24.
23 S. Groni, C. Hureau, R. Guillot, G. Blondin, G. Blain and E. Anxolabéhère-Mallart, *Inorg. Chem.*, 2008, **47**, 11783–11797.
24 M.-N. Collomb and A. Deronzier, *Eur. J. Inorg. Chem.*, 2009, 2025–2046.
25 C. Baffert, S. Dumas, J. Chauvin, J.-C. Leprêtre, M.-N. Collomb and A. Deronzier, *Phys. Chem. Chem. Phys.*, 2005, **7**, 202–210.
26 G. Eilers, C. Zettersten, L. Nyholm, L. Hammarström and R. Lomoth, *Dalton Trans.*, 2005, 1033–1041.

27 It should be pointed out that bubble formation makes an exact evaluation of the rates using this method difficult, therefore the rates reported should be considered for comparisons between complexes **1**–**4** only.
28 The authors are aware that small amounts of MnO_2 (a possible degradation product of **1**) could be responsible for the H_2O_2 disproportionation. However, this explanation is considered unlikely given that the rate of oxygen evolution followed first order kinetics over the concentration interval investigated and that the EPR showed no signs of degradation during the reactions.
29 G. S. Waldo and J. E. Penner-Hahn, *Biochemistry*, 1995, **34**, 1507–1512.
30 J. A. Lessa, A. Horn Jr., É. S. Bull, M. R. Rocha, M. Benassi, R. R. Catharino, M. N. Eberlin, A. Casellato, C. J. Noble, G. R. Hanson, G. Schenk, G. C. Silva, O. A. C. Antunes and C. Fernandes, *Inorg. Chem.*, 2009, **48**, 4569–4579.
31 W. L. F. Armarego and C. L. L. Chai, *Purification of Laboratory Chemicals*, 5th edn, Butterworth-Heinemann, Elsevier, Burlington, MA, 2003.
32 G. M. Sheldrick, *Acta Crystallogr., Sect. A: Found. Crystallogr.*, 2008, **64**, 112–122.
33 S. Brennan, CCP14 (Collaborative Computational Project No. 14), http://www.ccp14.ac.uk/ccp/ccp14/ftp-mirror/cross-section-sfac/pub/cross-section_codes/.
34 L. Kissel and R. H. Pratt, *Acta Crystallogr., Sect. A: Found. Crystallogr.*, 1990, **46**, 170–175.
35 J. Limburg, J. S. Vrettos, L. M. Liable-Sands, A. L. Rheingold, R. H. Crabtree and G. W. Brudvig, *Science*, 1999, **283**, 1524–1527.

